Research Article

Savas Evran* and Mustafa Kurt

CFD analysis of particle shape and Reynolds number on heat transfer characteristics of nanofluid in heated tube

https://doi.org/10.1515/phys-2024-0046
received March 14, 2024; accepted May 22, 2024

Abstract: Various nanoparticles have been used to increase the heat transfer characteristics (HTC) of nanofluids in the heated tube. The use of various shapes of the same nanoparticle can have major impact on the HTC. In this study, computational fluid dynamics (CFD) analysis of the impact of particle shape (Brick and Platelet) and Reynolds (Re) number (4,500, 6,000, 7,500, and 9,000) on the HTC of nanofluid in the heated tube was carried out in accordance with Taguchi method. Heat transfer coefficient, Nusselt (Nu) number, performance evaluation criteria, and average static pressure drop were chosen as HTC. CFD analyses for 1% Fe_3O_4 nanofluids in ANSYS Fluent software were performed in accordance with L8 orthogonal array. Particle shape and Re number were selected as the first and second factors, respectively. Signal/noise analysis was used to decide optimum levels and impact direction on HTC for each factor, whereas analysis of variance was implemented to define the importance levels and percentage impact ratios of the factors. According to the results obtained from the study, the nanofluids with platelet nanoparticles have a higher impact on the heat transfer coefficient compared to Brick nanoparticles. Although the increase in the Re number causes an increase in the heat transfer coefficient, Nu number, and average static pressure drop, it does not have any effect on the performance evaluation criteria. The results obtained from this study can be used as a guidance for experimental studies.

Keywords: ANOVA, CFD, heat transfer, nanofluids, Taguchi method

Nomenclature

b_l	base fluid
CFD	computational fluid dynamics
D_b	generation of turbulence kinetic energy due to buoyancy
D_k	generation of turbulence kinetic energy due to the mean velocity gradients
$\vec{F}$	external force
g	gravity
HTC	heat transfer characteristics
h	heat transfer coefficient
$\vec{J_j}$	diffusion flux
k_{eff}	effective conductivity
k	turbulence kinetic energy
Nu	Nusselt number
n_l	nanofluid
PEC	performance evaluation criteria
Q	heat transfer rate
Re	Reynolds number
S_h	energy source
S_k and S_ϵ	user defined source terms
S_m	source
S/N	signal/noise
T_i and T_o	inlet and outlet temperature
t	time
U	specific total energy
$\vec{v}$	velocity vector
ρ	fluid density
μ	viscosity
ϵ	rate of dissipation
σ_k	turbulent Prandtl numbers for k
$\bar{\bar{\tau}}$	stress tensor
Φ	volume fraction
σ_ε	turbulent Prandtl numbers for ε
μ_t	eddy viscosity
ΔP	pressure drop
$\tilde{\Omega}_{ij}$	mean rate-of-rotation tensor

*** Corresponding author: Savas Evran**, Faculty of Applied Sciences, Department of Jewelry and Jewelry Design, Marmara University, 34865, Istanbul, Turkey, e-mail: sevran@marmara.edu.tr
Mustafa Kurt: Faculty of Technology, Department of Mechanical Engineering, Marmara University, 34854, Istanbul, Turkey

1 Introduction

The energy needs may increase day by day in many industries and research has been carried out on carbon emissions and energy consumption [1]. Especially in heat energy, the usage of nanofluids has become extensive to increase efficiency. Many researchers [2,3] have analyzed improving the thermal conductivity by using nanofluids. Nanofluids are fluids made of nanoparticles such as metals, carbides, and ceramics using a base liquid [4,5]. Due to the several improved physical properties of nanofluids, they are subject to implementation in many sectors such as energy systems [6] and solar collectors [7], electronics cooling system [8], nuclear power plants [9], heat exchangers [10], microfluidics [11], enhanced oil recovery [12], impingement jets [13], renewable energy [14], combustions [15], porous media [16], *etc*. Different mathematical methods have been presented on the thermal conductivity of nanofluids and several approach and empirical relations were used for these methods [17,18]. Fe_3O_4 has been used as nanoparticle in many studies [19–21] to create nanofluids. Additionally, different nanoparticles such as Cu [22], Al_2O_3 [23], CuO [24], TiO_2 [25], ZnO [26], Ag [27], MWCNT [28], Ni [29], SiO_2 [30], ZrO_2 [31], CNT [32], and Au [33] have been the subject of many studies. Several research works have been done, such as improving performance and heat transfer, using nanofluids. Maddah *et al.* [34] examined the HTC of nanofluids and determined that thermal conductivity is affected by the change in volume fractions of the particles. They also found that Re number has key effects on the Nusselt (Nu) number and friction factor. Barik *et al.* [35] reported the impact of duct Re number on the heat transfer performances and decided that increasing duct Re number can also cause an increase in Nu number. Additionally, they detected that increasing nozzle Re number can also lead to a rise in pump power. They applied turbulent flow in the calculations. Mir *et al.* [36] examined the impact of volume fraction of nanoparticles on overall Nu number and determined that the rise in nanoparticle volume fraction can cause a rise in Nu number of nanofluids. In analysis, they applied Re numbers as 150, 300, 500, and 700. Zhang *et al.* [37] obtained nanofluids using Fe_3O_4 nanoparticles and water and they examined the variation among mass fraction and convective heat transfer for these nanofluids. They also discussed the trend among magnetic field and convective heat transfer. As an outcome of their studies, they found that the increase in Re number leads to an important increase in the convective heat transfer coefficient. Xuan and Li [38] examined the correlation among thermal conductivity and particle volume fraction for nanofluid formed in alumina–water system and found that the increase in volume fraction caused an increase in the thermal conductivity ratio. Additionally, many studies [39–45] have applied the Taguchi technique for various analyses of nanofluids. As literature research exhibits, many papers are related to heat transfer performance of nanofluids. Most of these studies have experimental and numerical approaches. However, studies with numerical, theoretical and statistical methods are very limited. In the numerical and statistical paper, the heat transfer characteristics (HTC) of nanofluids depending on various particle shapes and Re numbers were discussed using computational fluid dynamics (CFD) and Taguchi methods. The purpose for selecting various particle shapes in the analyses is to examine various thermal conductivity and viscosity for nanofluids. As understood in Table 4, the thermal conductivity and viscosity of the nanofluid including platelet nanoparticles is higher compared to the nanofluid including Brick nanoparticles. Thus, it can also explain the variations in the HTC of the nanofluid. Therefore, more effective HTC may be obtained by utilizing various shaped particle reinforcement for the same nanofluids. Additionally, ANOVA was implemented to govern the contribution fractions of the particle shape on the HTC. Thus, it may be easier to determine which factor has the maximum efficiency on the systems. With all these advantageous aspects, this study can support many contributions to the literature.

2 CFD analysis

CFD analyses for HTC of the nanofluids were carried out using ANSYS Fluent commercial software. In modelling, the pipe was used under the heat flux of 4,000 W/m^2. The heat flux was implemented homogeneously on the pipe wall surface. The pipe has a length of 1,000 mm and diameter of 15 mm. 3D computational domain was considered for the pipe flow. 3D domain for pipe in CFD analysis was illustrated in Figure 1.

In mesh processing, multi-zone method with free mesh type including hexa-dominant was applied. To ensure homogeneous distribution of the mesh process, face meshing process was applied to the inlet and outlet areas of the pipe. Additionally, inflation method was added. 2,544,000 elements and 2,571,569 nodes were used in the mesh process. Previous study shows that using 425,691 elements was sufficient for the Nu number and fraction factor [46]. Thus, the number of elements and nodes in this study were considered appropriate for mesh operations. Additionally, the enhanced wall treatment including pressure gradient and thermal effects was utilized. Absolute criteria for the continuity, x–y–z velocities, energy, k and epsilon were considered to be 10^{-6} and the hybrid method was employed for

solution initialization. The realizable k–ϵ approach in ANSYS Fluent was determined to be viscos model and this model can be stated as follows [47]:

$$\frac{\partial}{\partial t}(\rho k) + \frac{\partial}{\partial x_j}(\rho k u_j) = \frac{\partial}{\partial x_j}\left[\left(\mu + \frac{\mu_t}{\sigma_k}\right)\frac{\partial k}{\partial x_j}\right] + D_k + D_b - \rho\epsilon - Y_M + S_k, \tag{1}$$

$$\frac{\partial}{\partial t}(\rho\epsilon) + \frac{\partial}{\partial x_j}(\rho\epsilon u_j) = \frac{\partial}{\partial x_j}\left[\left(\mu + \frac{\mu_t}{\sigma_\epsilon}\right)\frac{\partial \epsilon}{\partial x_j}\right] + \rho C_1 S_\epsilon - \rho C_2 \frac{\epsilon^2}{k + \sqrt{\upsilon\epsilon}} + C_{1\epsilon}\frac{\epsilon}{k} C_{3\epsilon} G_b + S_\epsilon, \tag{2}$$

$$C_1 = \max\left[0.43, \frac{\eta}{\eta + 5}\right], \quad \eta = S\frac{k}{\epsilon}, \quad S = \sqrt{2S_{ij}S_{ij}}, \tag{3}$$

$$\mu_t = \rho C_\mu \frac{k^2}{\epsilon}, \tag{4}$$

$$C_\mu = \frac{1}{A_0 + A_s \frac{kU^*}{\epsilon}}, \tag{5}$$

$$U^* \equiv \sqrt{S_{ij}S_{ij} + \tilde{\Omega}_{ij}\tilde{\Omega}_{ij}}, \tag{6}$$

$$\tilde{\Omega}_{ij} = \Omega_{ij} - 2\epsilon_{ijk}\omega_k \qquad \Omega_{ij} = \bar{\Omega}_{ij} - \epsilon_{ijk}\omega_k, \tag{7}$$

$$A_0 = 4.04, \quad A_S = \sqrt{6}\cos\phi, \tag{8}$$

$$\phi = \frac{1}{3}\cos^{-1}(\sqrt{6}\,W) \qquad W = \frac{S_{ij}S_{jk}S_{ki}}{\tilde{S}^3} \qquad \tilde{S} = \sqrt{S_{ij}S_{ij}} \qquad S_{ij} = \frac{1}{2}\left(\frac{\partial u_j}{\partial x_i} + \frac{\partial u_i}{\partial x_j}\right), \tag{9}$$

$$C_{1\epsilon} = 1.44, \quad C_2 = 1.9, \quad \sigma_k = 1.0, \quad \sigma_\epsilon = 1.2. \tag{10}$$

Equations containing continuity, momentum, stress tensor, and energy for pipe flow in ANSYS commercial software can be calculated as follows, respectively [47]:

$$\frac{\partial \rho}{\partial t} + \nabla(\rho\vec{v}) = S_m, \tag{11}$$

$$\frac{\partial}{\partial t}(\rho\vec{v}) + \nabla(\rho\vec{v}\vec{v}) = -\nabla p + \nabla\bar{\bar{\tau}} + \rho\vec{g} + \vec{F}, \tag{12}$$

$$\bar{\bar{\tau}} = \mu\left[(\nabla\vec{v} + \nabla\vec{v}^T) - \frac{2}{3}\nabla\vec{v}I\right], \tag{13}$$

$$\frac{\partial(\rho U)}{\partial t} + \nabla.\,[\vec{v}(\rho U + p)] = \nabla.\left(k_{eff}\nabla T - \sum_j h_j\vec{J}_j + (\bar{\bar{\tau}}_{eff}.\,\vec{v})\right) + S_h. \tag{14}$$

3 Statistical analysis

In the statistical analyses, Taguchi method and ANOVA were statistically employed. L8 orthogonal array in Taguchi methodology was used for the grouping of various particle shape and Re number in CFD analyses. Two factors were determined in numerical modeling. The first factor has four levels, whereas the second factor has two levels. Re number was decided to be the first factor, whereas the particle shape was chosen as the second factor. Factors and their levels are established in Table 1.

One of the main purposes of this study is to determine the maximum data of the heat transfer characteristic such as heat transfer coefficient, Nu number, performance evaluation criteria (PEC), and average static pressure drop (ΔP). In this context, "Larger is Better" quality characteristic can be considered to achieve maximum responses. The equation for this quality characteristic can be explained as follows [48]:

$$(S/N)_{LB} \text{ for HTC} = -10\ \log\left[n^{-1}\sum_{i=1}^{n}(y_i^2)^{-1}\right]. \tag{15}$$

To detect the factors at the optimum levels and their influence directions on the heat transfer characteristic, analysis of signal-to-noise S/N ratio was statistically applied. Minitab R12 statistical program was implemented in all statistical determinations.

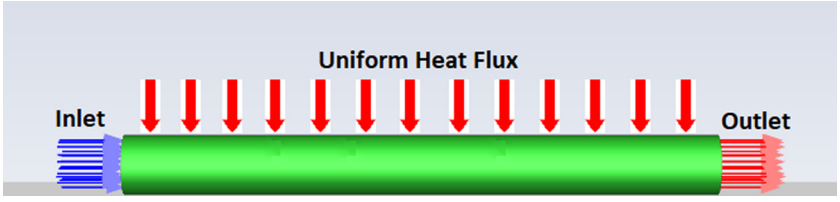

Figure 1: 3D domain for tube.

Table 1: Factors and levels in L8 orthogonal array

Factors	Icon	Levels			
		Level 1	Level 2	Level 3	Level 4
Re number	Re	4,500	6,000	7,500	9,000
Particle shape	PS	Brick	Platelet	—	—

4 Nanofluid analysis

In nanofluid characteristic, 1% Fe_3O_4 nanofluids were used. Nanoparticles have brick and platelet shapes in this study. In literature, nanoparticles with brick and platelet shapes have been limited, whereas shapes such as spherical, quasi-spherical, polyhedral, irregular, *etc.*, are generally common. Nanoparticles with different shapes can display various properties and these properties can play a key role on heat transfer characteristic. In the study, the nanofluids with 1% Fe_3O_4 nanoparticle was utilized and water was chosen to be the base fluid. Properties for water [49] and Fe_3O_4 nanoparticles [50] are exhibited in Table 2.

Volume fraction of nanoparticles in nanofluid can be expressed as follows [51]:

$$\varphi = \frac{V_{\mathrm{np}}}{V_{\mathrm{bl}} + V_{\mathrm{np}}}. \tag{16}$$

Density of the nanofluid may be determined as follows [52]:

$$\rho_{\mathrm{nl}} = \rho_{\mathrm{bl}}(1 - \varphi) + \varphi\rho_{\mathrm{np}}. \tag{17}$$

Specific heat in the nanofluid may be calculated as follows [53]:

$$C_{\mathrm{p,nl}} = \frac{(1 - \varphi)\rho_{\mathrm{bl}}C_{\mathrm{p,bl}} + \varphi\rho_{\mathrm{np}}C_{\mathrm{p,np}}}{\rho_{\mathrm{nl}}}. \tag{18}$$

Thermal conductivity in the nanofluid may be evaluated as follows [54]:

$$\frac{\mathrm{k_{nl}}}{\mathrm{k_l}} = \frac{\mathrm{k_p} + (n - 1)\mathrm{k_l} + (n - 1)(\mathrm{k_p} - \mathrm{k_l})\varphi}{(n - 1)\mathrm{k_l} - (\mathrm{k_p} - \mathrm{k_l})\varphi + \mathrm{k_p}}. \tag{19}$$

Table 2: Properties for base fluid and nanoparticle

Properties	Symbol	Unit	Base fluid [49]	Nanoparticle [50]
			Water	Fe_3O_4
Density	ρ	kg/m^3	998.2	5,200
Specific heat	C_p	J/kg K	4,180	670
Thermal conductivity	k	W/m K	0.6	6
Viscosity	μ	kg/ms	0.001003	—

Viscosity of the nanofluid can be solved as follows [55]:

$$\mu_{\mathrm{nl}} = \mu_{\mathrm{bl}}(1 + A_1\varphi + A_2\varphi^2). \tag{20}$$

Constants in accordance with thermal conductivity and viscosity based on the nanoparticle shapes are described in Table 3 [54].

The properties of the nanofluid were found using Eqs (16)–(20) and the results considered are established in Table 4.

As can be understood from Table 3, although the nanoparticle shape does not have any impact in the density and specific heat of the nanofluids, it plays a dominant role on thermal conductivity and viscosity. Therefore, variations that may occur in the HTC can be detected in accordance with the thermal conductivity and viscosity of the nanofluids.

5 HTC analysis

In the presented work, the influence of particle shape and Re number on the heat transfer coefficient (h), Nu number, PEC, and ΔP of nanofluid in heated pipe was analyzed as numerically and statistically. Four different Re numbers were considered in the analyses. Re number may be evaluated as follows [56]:

$$\mathrm{Re} = \frac{\rho VR}{\mu}. \tag{21}$$

Heat transfer coefficient in nanofluid may be solved as follows [56]:

$$h = \frac{Q}{A(T_{\mathrm{s}} - T_{\mathrm{l,ave}})}. \tag{22}$$

Heat transfer rate for nanofluid in pipe may be described as follows [56]:

$$Q = m_{\mathrm{l}}c_{\mathrm{p}}(T_{\mathrm{o}} - T_{\mathrm{i}}). \tag{23}$$

Nu number of nanofluid may be evaluated as follows [56]:

$$\mathrm{Nu} = \frac{hR}{k}. \tag{24}$$

PEC can be solved as follows [46,57]:

Table 3: Constants for nanoparticles [54]

Nanoparticle shape	N	A_1	A_2
Brick	3.7	1.9	471.4
Platelet	5.7	37.1	612.6

Table 4: Properties for nanofluids

Nanofluid	Nanoparticle shape	Density (kg/m^3)	Specific heat (J/kg K)	Thermal conductivity (W/m K)	Viscosity (kg/m s)
1 vol% Fe_3O_4/water	Brick	1040.218	4004.537	0.615844	0.001069
	Platelet	1040.218	4004.537	0.621068	0.001437

Table 5: CFD results for L8 orthogonal array

Test	Designation	Factors		CFD results			
		Re	PS	h (W/m^2 K)	Nu (−)	PEC (−)	ΔP (Pa)
1	Re_1PS_1	4,500	Brick	1671.9	40.722	0.998	159.44
2	Re_1PS_2	4,500	Platelet	1902.2	45.942	1.128	287.69
3	Re_2PS_1	6,000	Brick	2116.8	51.558	0.998	253.88
4	Re_2PS_2	6,000	Platelet	2409.3	58.189	1.128	458.13
5	Re_3PS_1	7,500	Brick	2547.3	62.044	0.998	366.31
6	Re_3PS_2	7,500	Platelet	2900.6	70.055	1.128	661.06
7	Re_4PS_1	9,000	Brick	2966.5	72.254	0.998	495.77
8	Re_4PS_2	9,000	Platelet	3379.0	81.609	1.128	894.73
Overall mean value				2486.7	60.297	1.063	447.13

$$\mathrm{PEC} = \frac{(\mathrm{Nu}_{\mathrm{nl}}/\mathrm{Nu}_{\mathrm{bl}})}{(f_{\mathrm{nl}}/f_{\mathrm{bl}})^{\frac{1}{3}}}. \tag{25}$$

Pressure drop in accordance with inner pressure and outer pressure can be found as follows [56]:

$$\Delta P = P_{\mathrm{i}} - P_{\mathrm{o}}. \tag{26}$$

6 Results and discussion

This CFD and statistical study is concerned about the evaluation of influence of particle shape and Re number on the h, Nu number, PEC, and ΔP of nanofluid in heated pipe. CFD analyses for 1% Fe_3O_4 nanofluids were carried out in accordance with the L8 orthogonal array and mathematical results achieved are presented in Table 5.

As described in Table 5, overall mean values of h, Nu number, PEC, and ΔP were calculated to be 2486.7 W/m^2 K, 60.297, 1.063, and 447.13 Pa, respectively. S/N ratios corresponding to CFD results based on "the Larger is better" quality characteristic are described in Table 6.

Velocity and temperature contours of CFD results using L8 orthogonal approach in Taguchi methodology are presented in Figures 2 and 3, respectively.

As understood from Figure 2, the velocity of the nanofluid rises from the pipe walls to the center of the pipe. This finding can be described by the resistance of the fluid against the pipe walls. As defined in Figure 3, the nanofluid temperature reduces from the pipe walls to the pipe center. This finding can be clarified by the temperature occurring on the pipe walls by the heat flux data. Temperature of pipe walls is high, whereas the temperature

Table 6: S/N ratios of CFD results for L8 orthogonal array

Test	Designation	Factors		S/N ratios (dB)			
		Re	PS	η for h	η for Nu	η for PEC	η for ΔP
1	Re_1PS_1	4,500	Brick	64.4642	32.1966	−0.0169	44.0519
2	Re_1PS_2	4,500	Platelet	65.5851	33.2442	1.0464	49.1785
3	Re_2PS_1	6,000	Brick	66.5136	34.2460	−0.0198	48.0926
4	Re_2PS_2	6,000	Platelet	67.6378	35.2969	1.0468	53.2198
5	Re_3PS_1	7,500	Brick	68.1216	35.8540	−0.0194	51.2770
6	Re_3PS_2	7,500	Platelet	69.2498	36.9088	1.0434	56.4048
7	Re_4PS_1	9,000	Brick	69.4449	37.1773	−0.0200	53.9056
8	Re_4PS_2	9,000	Platelet	70.5758	38.2348	1.0428	59.0338

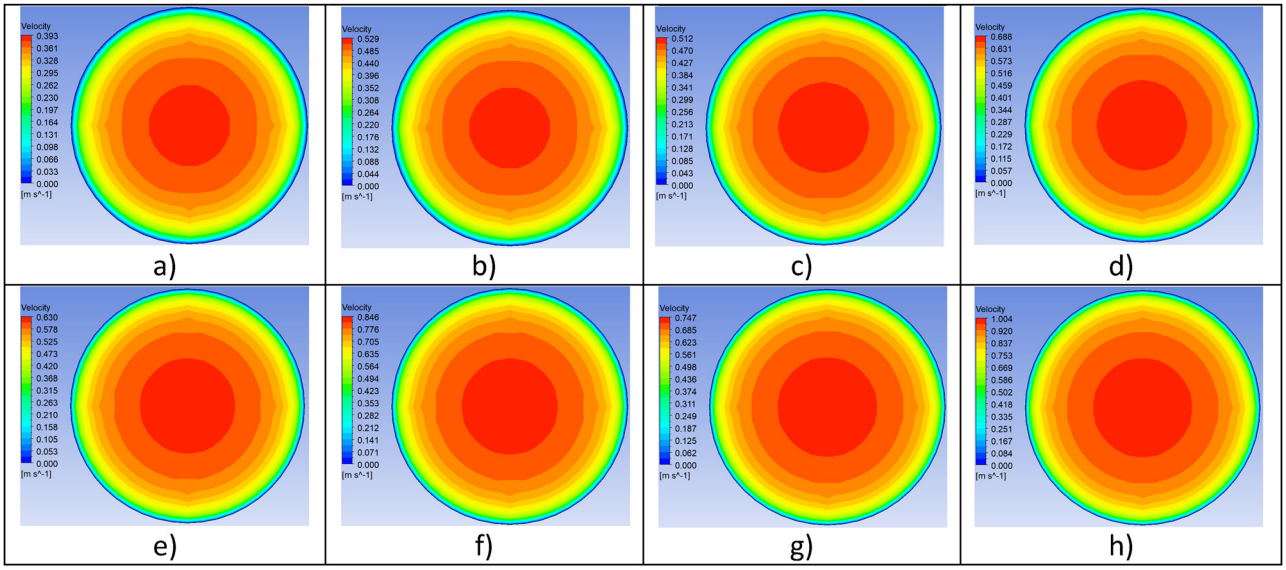

Figure 2: CFD velocity contour plots for (a) Re_1PS_1, (b) Re_1PS_2, (c) Re_2PS_1. (d) Re_2PS_2, (e) Re_3PS_1, (f) Re_3PS_2, (g) Re_4PS_1, (h) Re_4PS_2.

decreases towards the center of the pipe. Thus, difference was detected in temperature distribution due to the nanofluid.

6.1 Effect on HTC

To understand the influence of particle shape and Re number on the HTC of nanofluids, CFD analyses were carried out using various levels of different factors. The numerical results achieved by ANSYS Fluent software were evaluated as *S*/*N* ratio values to obtain the maximum HTC of nanofluids. Average CFD data corresponding to average *S*/*N* ratios were used to define the impact of each particle shape and Re number on the HTC at various levels. Graphs were drawn based on the *S*/*N* ratios. Impact of particle shape and Re number on the HTC of nanofluids are displayed in Figure 4.

Figure 4a–d displays that nanofluids containing 1% Fe_3O_4 nanoparticles with platelet shape have a higher influence on the *h*, Nu number, PEC, and Δ*P* compared to brick nanoparticles. This finding may be defined by thermal conductivity and viscosity. This situation is clearly determined in Eqs (19) and (20). The thermal conductivity and viscosity for

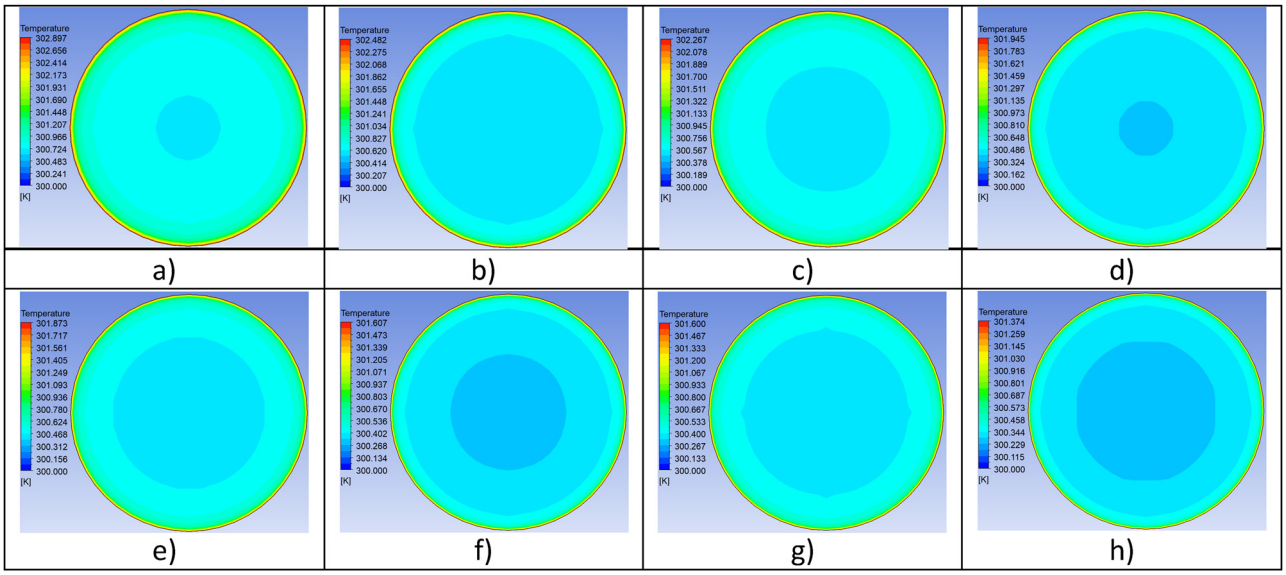

Figure 3: CFD temperature contour plots for (a) Re_1PS_1, (b) Re_1PS_2, (c) Re_2PS_1, (d) Re_2PS_2, (e) Re_3PS_1, (f) Re_3PS_2, (g) Re_4PS_1, (h) Re_4PS_2.

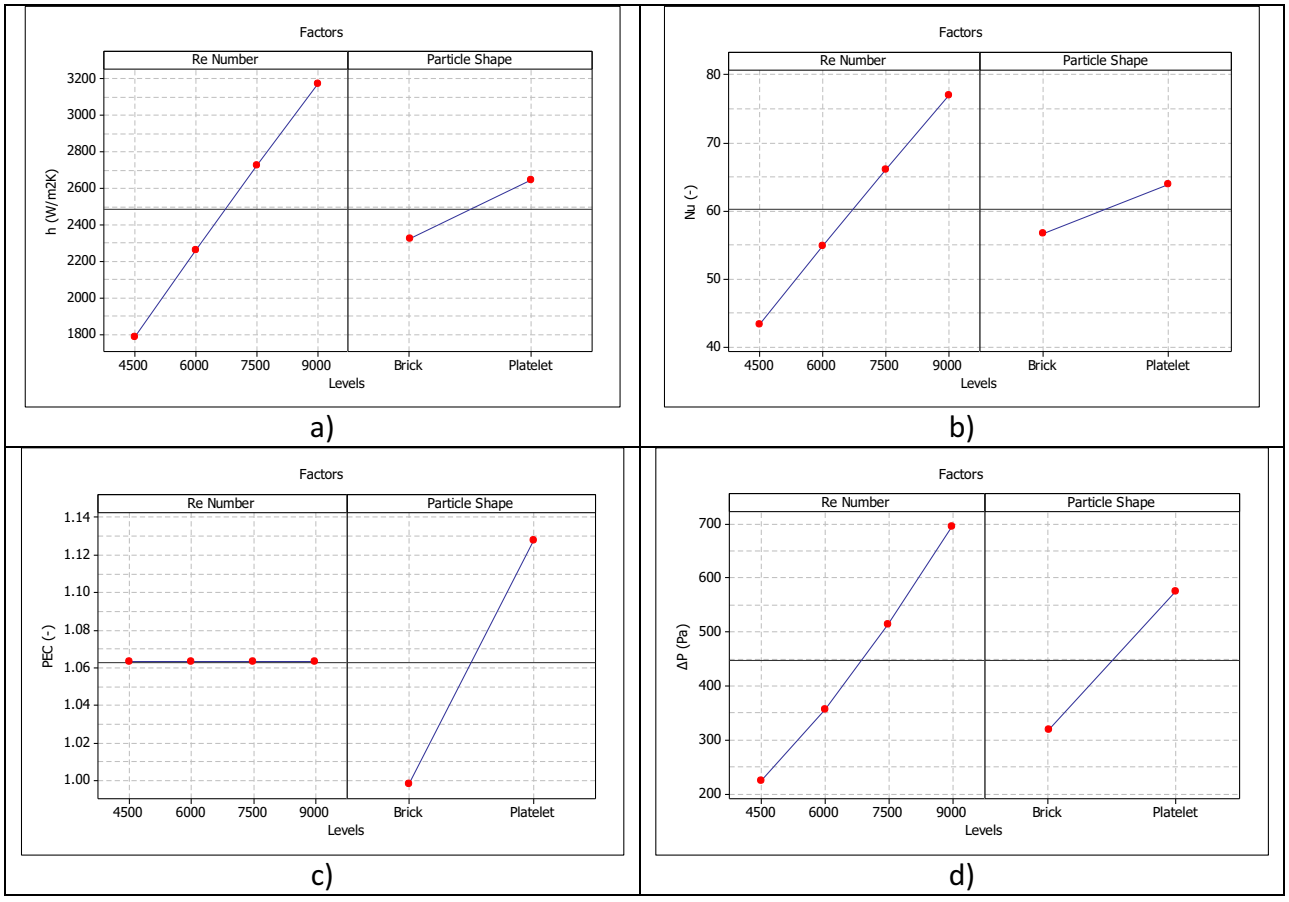

Figure 4: Main impact plots for (a) h, (b) Nu number, (c) PEC, (d) ΔP.

nanofluid including platelet nanoparticle are greater than nanofluid with brick nanoparticle. The increase in thermal conductivity of nanofluids causes an increase in the h, Nu number, and PEC. Although the increase in the Re number from 4,500 to 9,000 leads to an increase in the h, Nu number, and ΔP, it does not have any effect on the PEC. These findings were supported by the study by Garud and Lee [46]. Additionally, another study [58] showed that increasing Re number causes an increase in h, Nu number, and ΔP.

6.2 Optimal levels of particle shape and Re number

ANOVA is one of the statistical methods and it was employed to define the HTC. ANOVA was implemented to achieve the significance level and percent contribution ratio of particle shape and Re number on the HTC of nanofluids. Analyses were implemented in accordance with 95% confidence level. ANOVA results for h and Nu number are shown in Table 7.

According to the F-test results in Table 5, particle shape and Re number were determined as the most important factors on the heat transfer coefficient. Additionally, Re number has a 90.77% impact on h, whereas particle shape has 8.83% effect. This finding shows that Re number is dominant on h and Nu number compared to the particle shape. For the Nu number, particle shape and Re number were considered as important factors based on F-test results. Re number has a 91.84% influence on the Nu number, whereas particle shape has 7.81% effect. This finding indicates that the influence of turbulent flow on Nu number is more dominant compared to the particle shape. ANOVA outcomes for the PEC and average static pressure drop are displayed in Table 8.

ANOVA results in Table 6 show that Re number has no impact on the PEC. But, the impact of particle shape is great. Thus, the denominator of F-test was calculated as zero for the PEC. According to this outcome, the one major factor was determined to be the particle shape. Therefore, the particle shape of nanoparticle has a 100% influence on PEC, whereas RE number has a 0% influence. According to

Table 7: ANOVA for *h* and Nu

Source	DF	*h*					Nu				
		Seq SS	Adj MS	*F*	*P*	% Effect	Seq SS	Adj MS	*F*	*P*	% Effect
Re	3	2,132,963	710,988	231.23	0	90.77	1254.05	418.02	263.94	0	91.84
PS	1	207,561	207,561	67.50	0.004	8.83	106.70	106.70	67.37	0.004	7.81
Error	3	9,224	3,075			0.39	4.75	1.58			0.35
Total	7	2,349,749				100	1365.5				100
R^2 = 99.61% and R^2 (adj) = 99.08							R^2 = 99.65% and R^2 (adj) = 99.19%				

Table 8: ANOVA for PEC and Δ*P*

Source	DF	PEC					Δ*P*				
		Seq SS	Adj MS	*F*	*P*	% Effect	Seq SS	Adj MS	*F*	*P*	% Effect
Re	3	0	0	**	—	0	248,556	82,852	12.14	0.035	62.04
PS	1	0.0338	0.0338	**	—	100	131,638	131,638	19.29	0.022	32.86
Error	3	0	0		—	0	20,468	6,823			5.11
Total	7	0.0338				100	400,663				100
R^2 = 100.00% and R^2 (adj) = 100.00%							R^2 = 94.89% and R^2 (adj) = 88.08%				

the *F*-test results on the average static pressure drop, both particle shape and Re number were found to be important factors. According to the influence ratios, the Re number had a 62.04% influence on the average static pressure drop, whereas the particle shape had a 32.86% influence. This finding displays that the flow velocity in turbulent flow is greater than the effect of particle shape. The key purpose of the presented work is to determine the optimum levels of factors to obtain the highest HTC of nanofluids. In this context, the numerically calculated *h*, Nu number, PEC, and Δ*P* of nanofluid results were converted into *S*/*N* ratios. Average CFD results and *S*/*N* ratios were calculated for each level of particle shape and Re number. Overall CFD data and *S*/*N* ratios at all levels of particle shape and Re number according to *h* and Nu are exhibited in Table 9.

The overall results obtained from Table 9 display that the increase in Re number causes an increase in the *h* and Nu number. Thus, the particle with platelet shape had the optimum impact levels on the *h* and Nu number, whereas the optimum Re number was determined as 9,000. Therefore, to obtain the maximum *h* and Nu number, nanofluids including platelet nanoparticles and Re number of 9,000 should be determined. Average data of CFD and *S*/*N* ratios at all levels of particle shape and Re number in accordance with the PEC, and average static pressure drop of nanofluid are presented in Table 10.

The results shown in Table 10 exhibits that the nanofluids with platelet-shaped nanoparticles were determined as the optimum since the maximum PEC and static pressure drop were reached while using platelet-shaped

Table 9: Mean results for *h* and Nu

Level	*h*				Nu			
	S/*N* ratio (dB)		Mean value (W/m^2 K)		*S*/*N* ratio (dB)		Mean value	
	Re	PS	Re	PS	Re	PS	Re	PS
1	65.02	67.14	1,787	2326	32.72	34.87	43.33	56.64
2	67.08	68.26	2,263	2648	34.77	35.92	54.87	63.95
3	68.69		2,724		36.38		66.05	
4	70.01		3,173		37.71		76.93	
Delta	4.99	1.13	1,386	322	4.99	1.05	33.60	7.30
Rank	1	2	1	2	1	2	1	2

Table 10: Main results for PEC and Δ*P*

Level	PEC				Δ*P*			
	S/*N* ratio (dB)		Mean value		*S*/*N* ratio (dB)		Mean value (Pa)	
	Re	PS	Re	PS	Re	PS	Re	PS
1	0.51472	−0.01902	1.0630	0.9978	46.62	49.33	223.60	318.90
2	0.51349	1.04484	1.0629	1.1278	50.66	54.46	356.00	575.40
3	0.51200		1.0627		53.84		513.70	
4	0.51143		1.0626		56.47		695.30	
Delta	0.0033	1.06387	0.0004	0.1300	9.85	5.13	471.70	256.60
Rank	2	1	2	1	1	2	1	2

nanoparticles. Additionally, because no impact of Re number on the PEC was detected, the ideal level for Re number cannot be analyzed. It indicates that the increase in the Re number in the average static pressure drop leads to an increase in the pressure drop. Therefore, the ideal level for Re number on pressure drop was observed as 9,000. The maximum static pressure drop can be achieved by applying nanofluid including platelet nanoparticles and Re number of 9,000.

6.3 Estimation of optimal heat transfer responses

Particle shape and Re numbers at the optimal levels were selected to achieve the maximum HTC of nanofluids. *S*/*N* ratio analysis was applied to decide optimum levels and average results were evaluated. ANOVA was implemented and significant particle shape and Re number based on *F*-test results were discussed. Determination of predicted HTC regarding *S*/*N* ratio and ANOVA results at 95% confidence level can be solved as follows [48]:

$$\mu_{\text{est}} = \bar{\text{PS}}_{\text{opt}} + \bar{\text{Re}}_{\text{opt}} - \bar{T}_{\text{ave}}, \tag{27}$$

where $\bar{\text{PS}}_{\text{opt}}$ and $\bar{\text{Re}}_{\text{opt}}$ for the heat transfer coefficient were calculated as 3,173 and 2,648 W/m^2 K, whereas $\bar{\text{PS}}_{\text{opt}}$ and $\bar{\text{Re}}_{\text{opt}}$ for the Nusellt number were solved as 76.93 and 63.95, respectively. Additionally, $\bar{\text{PS}}_{\text{opt}}$ and $\bar{\text{Re}}_{\text{opt}}$ for the PEC were determined as 1.063 and 1.1278, whereas $\bar{\text{PS}}_{\text{opt}}$ and $\bar{\text{Re}}_{\text{opt}}$ for the average static pressure drop were found as 695.30 and 575.40 Pa, respectively. $\bar{T}_{\text{ave}}$ for the *h*, Nu number, PEC, and Δ*P* were calculated as 2486.7 W/m^2 K, 60.297, 1.063, and 447.13 Pa, respectively. These data are substituted in Eq. (27) and the predicted Taguchi results are exhibited in Table 11.

7 Validation

Numerical and statistical results of Nu number and PEC of nanofluids were compared with theoretical approach. In this context, Nu number and Darcy friction factor were solved theoretically. Calculations for validation were carried out for particle shape and Re numbers under the optimal levels. Theoretical Nu number and Darcy friction factors were considered using Eqs (28) [59] and (29) [60], respectively.

$$\bar{\text{Nu}}_R = 0.023\,\text{Re}^{0.8}\,\text{Pr}^{0.4}, \tag{28}$$

Table 12: Theoretical validation of CFD results

Nu (Re_4PS_2)		% Difference	PEC ($Re_{all}PS_2$)		% Difference
CFD	Formula		CFD	Formula	
81.609	81.624	0.02	1.128	1.132	0.35

Table 11: CFD and estimated optimal heat transfer responses

HTC	*h* (Re_4PS_2)	Nu (Re_4PS_2)	PEC ($Re_{all}PS_2$)	Δ*P* (Re_4PS_2)
CFD results	3379.0 W/m^2 K	81.609	1.128	894.73
Taguchi results	3334.3 W/m^2 K	80.583	1.128	823.57
% differences	1.32	1.16	0	7.95

$$\frac{1}{\sqrt{f}} = -2\log\left(\frac{e/R}{3.7} + \frac{2.52}{R_e\sqrt{f}}\right). \quad (29)$$

CFD, estimated Taguchi results, and theoretical results obtained for Nu number and PEC utilizing particle shape and Re number under the ideal levels are exhibited in Table 12.

Table 12 shows that while the difference among CFD and theoretical data of the Nu number was found to be 0.02%, the difference for the PEC was determined to be 0.35%. These findings prove the precision of the numerical and statistical data.

8 Conclusion

In the presented study, the impact of particle shape and Reynolds (Re) number on the h, Nu number, PEC, and ΔP of nanofluid in heated tube was analyzed in accordance with Taguchi method. Fe_3O_4 was selected as nanoparticle and so 1% Fe_3O_4 nanofluids for CFD analyses was used. Particle shape and Re number were assumed as the first and second factors. Brick and platelet were considered as particle shapes. CFD calculations for HTC of nanofluids were carried out by ANSYS Fluent commercial software regarding L8 orthogonal range utilizing Taguchi methodology. A pipe of 1,000 mm length and 15 mm diameter was implemented in numerical modeling. The heat flux was chosen as 4,000 W/m^2. S/N ratio analysis was implemented to find optimum levels and impact trend on HTC for each factor, whereas ANOVA was conducted to release the dominant levels and percentage impact rates of the factors. The key results obtained from this study are summarized below:

- Increasing Re number from 4,500 to 9,000 causes an increase in HTC of the nanofluid.
- The influence of platelet nanoparticles on the HTC of the nanofluid is greater than brick nanoparticles.
- The maximum heat transfer characteristic of the nanofluid is achieved by using platelet nanoparticles and Re number of 9,000.
- According to the F-test data in the ANOVA results, particle shape is detected as a significant factor. However, Re number was determined to be a significant factor on heat transfer coefficient, Nu number, and average static pressure drop, whereas no impact was found on the PEC.
- The contribution ratio of particle shape on the heat transfer coefficient, Nu number, PEC, and average static pressure drop is found to be 8.83, 7.81, 100, and 32.86%, respectively.
- The contribution ratio of Re number on heat transfer coefficient, Nu number, PEC, and average static pressure drop is decided to be 90.77, 91.84, 0, and 62.04%, respectively.
- The difference between numerical and Taguchi prediction results obtained for heat transfer coefficient, Nu number, performance evaluation criteria, and average static pressure drop was determined to be 1.32, 1.16, 0, and 7.95%, respectively.
- In the validation calculations, the difference between the CFD and theoretical results for the Nu number was found to be 0.02%, whereas the difference between the CFD and theoretical data obtained for the performance evaluation criteria was solved to be 0.35%.
- The temperature of the nanofluid reduces from the pipe walls to the center of the pipe, whereas the nanofluid velocity increases from the pipe walls to the center.

Funding information: The authors state no funding involved.

Author contributions: All authors have accepted responsibility for the entire content of this manuscript and approved its submission.

Conflict of interest: The authors state no conflict of interest.

References

[1] Waheed R, Sarwar S, Wei C. The survey of economic growth, energy consumption and carbon emission. Energy Rep. 2019;5:1103–15.
[2] Indhuja A, Suganthi K, Manikandan S, Rajan K. Viscosity and thermal conductivity of dispersions of gum arabic capped MWCNT in water: Influence of MWCNT concentration and temperature. J Taiwan Inst Chem Eng. 2013;44:474–9.
[3] Yu W, Xie H, Chen L, Li Y. Enhancement of thermal conductivity of kerosene-based Fe_3O_4 nanofluids prepared via phase-transfer method. Colloids Surf A: Physicochem Eng Asp. 2010;355:109–13.
[4] Lenin R, Joy PA, Bera C. A review of the recent progress on thermal conductivity of nanofluid. J Mol Liq. 2021;338:116929.
[5] Sajid MU, Ali HM. Thermal conductivity of hybrid nanofluids: a critical review. Int J Heat Mass Transf. 2018;126:211–34.
[6] Cuce E, Cuce PM, Guclu T, Besir AB. On the use of nanofluids in solar energy applications. J Therm Sci. 2020;29:513–34.
[7] Yousefi T, Veysi F, Shojaeizadeh E, Zinadini S. An experimental investigation on the effect of Al_2O_3-H_2O nanofluid on the efficiency of flat-plate solar collectors. Renew Energy. 2012;39:293–8.
[8] Sohel M, Saidur R, Khaleduzzaman S, Ibrahim TA. Cooling performance investigation of electronics cooling system using Al_2O_3–H_2O nanofluid. Int Commun Heat Mass Transf. 2015;65:89–93.
[9] Bafrani HA, Noori-kalkhoran O, Gei M, Ahangari R, Mirzaee MM. On the use of boundary conditions and thermophysical properties of nanoparticles for application of nanofluids as coolant in nuclear

power plants; a numerical study. Prog Nucl Energy. 2020;126:103417.
[10] Pandya NS, Shah H, Molana M, Tiwari AK. Heat transfer enhancement with nanofluids in plate heat exchangers: A comprehensive review. Eur J Mech-B/Fluids. 2020;81:173–90.
[11] Yi P, Kayani AA, Chrimes AF, Ghorbani K, Nahavandi S, Kalantar-Zadeh K, et al. Thermal analysis of nanofluids in microfluidics using an infrared camera. Lab a Chip. 2012;12:2520–5.
[12] Li K, Wang D, Jiang S. Review on enhanced oil recovery by nanofluids. Oil Gas Sci Technol–Revue d'IFP Energies nouvelles. 2018;73:37.
[13] Balla HH, Hashem AL, Kareem ZS, Abdulwahid AF. Heat transfer potentials of ZnO/water nanofluid in free impingement jet. Case Stud Therm Eng. 2021;27:101143.
[14] Singh T, Atieh MA, Al-Ansari T, Mohammad AW, McKay G. The role of nanofluids and renewable energy in the development of sustainable desalination systems: A review. Water. 2020;12:2002.
[15] Jadeja KM, Bumataria R, Chavda N. Nanofluid as a coolant in internal combustion engine–a review. Int J Ambient Energy. 2023;44:363–80.
[16] Esfe MH, Bahiraei M, Hajbarati H, Valadkhani M. A comprehensive review on convective heat transfer of nanofluids in porous media: Energy-related and thermohydraulic characteristics. Appl Therm Eng. 2020;178:115487.
[17] Patel HE, Anoop K, Sundararajan T, Das SK. A micro-convection model for thermal conductivity of nanofluids. International Heat Transfer Conference 13. Begel House Inc.; 2006.
[18] Chon CH, Kihm KD, Lee SP, Choi SU. Empirical correlation finding the role of temperature and particle size for nanofluid (Al_2O_3) thermal conductivity enhancement. Appl Phys Lett. 2015;65:89–93.
[19] Ebaid MS, Ghrair AM, Al-busoul M. Investigation of heat transfer enhancement using ferro-nanofluids (Fe_3O_4/water) in a heated pipe under the application of magnetic field. Adv Mech Eng. 2022;14:16878132221102647.
[20] Kichatov B, Korshunov A, Sudakov V, Golubkov A, Kolobov A, Chikishev L. Magnetic nanofluid Fe_3O_4 in passive cooling system based on thermo-osmotic effect. Int J Therm Sci. 2024;199:108931.
[21] Afshari F, Muratçobanoğlu B. Thermal analysis of Fe_3O_4/water nanofluid in spiral and serpentine mini channels by using experimental and theoretical models. Int J Environ Sci Technol. 2023;20:2037–52.
[22] Khamliche T, Khamlich S, Moodley M, Mothudi B, Henini M, Maaza M. Laser fabrication of Cu nanoparticles based nanofluid with enhanced thermal conductivity: Experimental and molecular dynamics studies. J Mol Liq. 2021;323:114975.
[23] Kong M, Lee S. Performance evaluation of Al_2O_3 nanofluid as an enhanced heat transfer fluid. Adv Mech Eng. 2020;12:1687814020952277.
[24] Nfawa SR, Basri AA, Masuri SU. Novel use of MgO nanoparticle additive for enhancing the thermal conductivity of CuO/water nanofluid. Case Stud Therm Eng. 2021;27:101279.
[25] Hozien O, El-Maghlany WM, Sorour MM, Mohamed YS. Experimental study on thermophysical properties of TiO_2, ZnO and Ag water base nanofluids. J Mol Liq. 2021;334:116128.
[26] Azeez K, Ibrahim ZA, Hussein AM. Thermal conductivity and viscosity measurement of ZnO nanoparticles dispersing in various base fluids. J Adv Res Fluid Mech Therm Sci. 2020;66:1–10.
[27] Pourrajab R, Noghrehabadi A, Behbahani M, Hajidavalloo E. An efficient enhancement in thermal conductivity of water-based hybrid nanofluid containing MWCNTs-COOH and Ag nanoparticles: experimental study. J Therm Anal Calorim. 2021;143:3331–43.
[28] Lyu Z, Asadi A, Alarifi IM, Ali V, Foong LK. Thermal and fluid dynamics performance of MWCNT-water nanofluid based on thermophysical properties: an experimental and theoretical study. Sci Rep. 2020;10:5185.
[29] Saleh B, Sundar LS. Experimental study on heat transfer, friction factor, entropy and exergy efficiency analyses of a corrugated plate heat exchanger using Ni/water nanofluids. Int J Therm Sci. 2021;165:106935.
[30] Zhang L, Zhang A, Jing Y, Qu P, Wu Z. Effect of particle size on the heat transfer performance of SiO_2–water nanofluids. J Phys Chem C. 2021;125:13590–600.
[31] Kolappan S, Karthik S, Logesh K, Vasudevan A. Thermal characterisation study of ZrO_2/water nanofluid. Int J Ambient Energy. 2020;41:918–21.
[32] Yadav D, Sanserwal M. A comprehensive review of the effects of various factors on the thermal conductivity and rheological characteristics of CNT nanofluids. J Therm Anal Calorim. 2023;148:1723–63.
[33] Ternik P. Conduction and convection heat transfer characteristics of water–Au nanofluid in a cubic enclosure with differentially heated side walls. Int J Heat Mass Transf. 2015;80:368–75.
[34] Maddah H, Alizadeh M, Ghasemi N, Alwi SRW. Experimental study of Al_2O_3/water nanofluid turbulent heat transfer enhancement in the horizontal double pipes fitted with modified twisted tapes. Int J Heat Mass Transf. 2014;78:1042–54.
[35] Barik AK, Rout S, Mukherjee A. Numerical investigation of heat transfer enhancement from a protruded surface by cross-flow jet using Al_2O_3–water nanofluid. Int J Heat Mass Transf. 2016;101:550–61.
[36] Mir S, Akbari OA, Toghraie D, Sheikhzadeh G, Marzban A, Mir S, et al. A comprehensive study of two-phase flow and heat transfer of water/Ag nanofluid in an elliptical curved minichannel. Chin J Chem Eng. 2020;28:383–402.
[37] Zhang R, Qing S, Zhang X, Li J, Liu Y, Wen X. Experimental investigation and machine learning modeling of heat transfer characteristics for water based nanofluids containing magnetic Fe_3O_4 nanoparticles. Mater Today Commun. 2023;36:106798.
[38] Xuan Y, Li Q. Heat transfer enhancement of nanofluids. Int J Heat Fluid Flow. 2000;21:58–64.
[39] Mohammadi M, Abadeh A, Nemati-Farouji R, Passandideh-Fard M. An optimization of heat transfer of nanofluid flow in a helically coiled pipe using Taguchi method. J Therm Anal Calorim. 2019;138:1779–92.
[40] Raei B. Statistical analysis of nanofluid heat transfer in a heat exchanger using Taguchi method. J Heat Mass Transf Res. 2021;8:29–38.
[41] Sobhani M, Ajam H. Taguchi optimization for natural convection heat transfer of Al_2O_3 nanofluid in a partially heated cavity using LBM. J Therm Anal Calorim. 2019;138:889–904.
[42] Zahmatkesh I, Shandiz MRH. Optimum constituents for MHD heat transfer of nanofluids within porous cavities: A Taguchi analysis in natural and mixed convection configurations. J Therm Anal Calorim. 2019;138:1669–81.
[43] Bazkhane S, Zahmatkesh I. Taguchi-based sensitivity analysis of hydrodynamics and heat transfer of nanofluids in a microchannel heat sink (MCHS) having porous substrates. Int Commun Heat Mass Transf. 2020;118:104885.

[44] Javadpour SM, Abadi EAJ, Akbari OA, Goharimanesh M. Optimization of geometry and nano-fluid properties on micro-channel performance using Taguchi method and genetic algorithm. Int Commun heat mass Transf. 2020;119:104952.
[45] Gelis K, Ozbek K, Ozyurt O, Celik AN. Multi-objective optimization of a photovoltaic thermal system with different water based nanofluids using Taguchi approach. Appl Therm Eng. 2023;219:119609.
[46] Garud KS, Lee M-Y. Numerical investigations on heat transfer characteristics of single particle and hybrid nanofluids in uniformly heated tube. Symmetry. 2021;2–19.
[47] ANSYS. ANSYS FLUENT 12.0 Theory Guide. Inc, Canonsburg, PA; 2009.
[48] Ross PJ. Taguchi techniques for quality engineering: McGraw-Hill International Editions. 2nd edn. New York, USA; 1996.
[49] Chaurasia SR, Sarviya RM. Comparative thermal performance analysis with entropy generation on helical screw insert in tube with number of strips with nanofluid at laminar flow regime. Int Commun Heat Mass Transf. 2021;122:105138.
[50] Sheikholeslami M, Shehzad SA. CVFEM for influence of external magnetic source on Fe_3O_4-H_2O nanofluid behavior in a permeable cavity considering shape effect. Int J Heat Mass Transf. 2017;115:180–91.
[51] Khanafer K, Vafai K. A critical synthesis of thermophysical characteristics of nanofluids. Int J Heat Mass Transf. 2011;54:4410–28.
[52] Pak BC, Cho YI. Hydrodynamic and heat transfer study of dispersed fluids with submicron metallic oxide particles. Exp Heat Transf. 1998;11:151–70.
[53] Xuan Y, Roetzel W. Conceptions for heat transfer correlation of nanofluids. Int J heat Mass Transf. 2000;43:3701–7.
[54] Timofeeva EV, Routbort JL, Singh D. Particle shape effects on thermophysical properties of alumina nanofluids. J Appl Phys. 2009;106:1–10.
[55] Rudyak V, Belkin AA, Tomilina EA, Egorov VV. Nanoparticle Friction Force and Effective Viscosity of Nanosuspensions. Defect Diffus Forum. 2008;273-276:566–71.
[56] Mauri R. Transport phenomena in multiphase flows. Switzerland: Springer; 2015.
[57] Singh SK, Sarkar J. Thermohydraulic behavior of concentric tube heat exchanger inserted with conical wire coil using mono/hybrid nanofluids. Int Commun Heat Mass Transf. 2021;122:105134.
[58] Saedodin S, Zaboli M, Rostamian SH. Effect of twisted turbulator and various metal oxide nanofluids on the thermal performance of a straight tube: Numerical study based on experimental data. Chem Eng Process - Process Intensif. 2020;158:108106.
[59] Balaji C, Srinivasan B, Gedupudi S. Heat transfer engineering: fundamentals and techniques. London: Academic Press; 2020.
[60] Cengel Y, Cimbala J. Fluid mechanics fundamentals and applications. 3rd edn. New York: McGraw Hill; 2014.